# Broadband adiabatic inversion pulses for cross polarization in wideline solid-state NMR spectroscopy

Kristopher J. Harris [a], Adonis Lupulescu [b], Bryan E.G. Lucier [a], Lucio Frydman [b],*, Robert W. Schurko [a],*

[a] Department of Chemistry, University of Windsor, 401 Sunset Avenue, Windsor, Ontario, Canada N9B 3P4
[b] Department of Chemical Physics, Weizmann Institute of Science, 76100 Rehovot, Israel

## ABSTRACT

Efficient acquisition of ultra-wideline solid-state NMR powder patterns is a continuing challenge. In particular, when the breadth of the powder pattern is much larger than the cross-polarization (CP) excitation bandwidth, transfer efficiencies suffer and experimental times are greatly increased. Presented herein is a CP pulse sequence with an excitation bandwidth that is up to ten times greater than that available from a conventional spin-locked CP pulse sequence. The pulse sequence, *b*roadband *a*diabatic *in*version CP (BRAIN-CP), makes use of the broad, uniformly large frequency profiles of chirped inversion pulses, to provide these same characteristics to the polarization transfer process. A detailed theoretical analysis is given, providing insight into the polarization transfer process involved in BRAIN-CP. Experiments on spin-1/2 nuclei including $^{119}$Sn, $^{199}$Hg and $^{195}$Pt nuclei are presented, and the large bandwidth improvements possible with BRAIN-CP are demonstrated. Furthermore, it is shown that BRAIN-CP can be combined with broadband frequency-swept versions of the Carr–Purcell–Meiboom–Gill experiment (for instance with WURST–CPMG, or WCPMG for brevity); the combined BRAIN-CP/WCPMG experiment then provides multiplicative signal enhancements of both CP and multiple-echo acquisition over a broad frequency region.

© 2012 Elsevier Inc. All rights reserved.

## 1. Introduction

Solid-state nuclear magnetic resonance (NMR) spectroscopy has become a widely used technique for the characterization of atomic-level structure and dynamics, largely because of the extreme sensitivity of the NMR interactions to the local environment of each nucleus [1,2]. In many such instances, the anisotropic character of the chemical shift and/or quadrupolar interactions can lead to NMR powder patterns possessing spectral breadths ranging from hundreds of kHz to several MHz. Unfortunately, experimental difficulties associated with acquiring such broad, ultra-wideline (UW) powder patterns can prevent the determination of the NMR parameters and the detailed chemical information they encode. Development of specialized techniques and hardware for the acquisition of UW NMR spectra to provide detailed structural information on new materials has accordingly been the subject of intensive research efforts [3].

Because the dispersion of spectral intensity over a large frequency region leads to a reduction in the signal-to-noise ratio (S/N), methods for increasing the signal strength are often required in UW NMR spectroscopy. One technique for enhancing the S/N relies on preservation of the observable transverse-plane NMR signal, by applying a series of refocusing pulses, following the method of Carr and Purcell [4] and Meiboom and Gill [5] (CPMG). The CPMG method has proven to be extremely useful for acquiring wideline spectra of both spin-1/2 and quadrupolar (spin > ½) nuclei [6,7]. When the effective bandwidth of the pulses or of the probe electronics is insufficient, the powder pattern can be mapped out with a series of acquisitions at different transmitter frequencies [8,9]. Broadband frequency-swept pulses are also capable of exciting spin echoes [10–13]; for instance, it has recently been shown that a CPMG echo train can be acquired using *w*ideband, *u*niform *r*ate, *s*mooth *t*runcation (WURST) pulses [14]. The ensuing WURST–CPMG (WCPMG for brevity) pulse sequence enables extremely broad frequency ranges to be observed simultaneously, providing the S/N advantage of a CPMG-like echo train in experiments involving both spin-½ and quadrupolar nuclei [15,16].

Cross-polarization (CP) is another S/N-enhancing technique that is applied extensively in solids NMR spectroscopy [17–19]. The transfer of polarization affords S/N gains from proximate higher-$\gamma$ nuclei. A further advantage over direct excitation methods often results from the faster repetition rates associated with the

---

* Corresponding authors.
  *E-mail addresses:* lucio.frydman@weizmann.ac.il (L. Frydman), rschurko@uwindsor.ca (R.W. Schurko).

generally much shorter longitudinal relaxation times ($T_1$'s) of the high-$\gamma$ nuclei. Unfortunately, the bandwidth over which CP is effective is often determined by the strength of the spin-locking fields employed, and the resultant excitation covers only a small fraction of the total NMR powder pattern when large anisotropic NMR interactions are present. Therefore, once again, either stepwise acquisition or broadband direct excitation methods must be employed, leading to lengthy total experimental times. The recent availability of commercial ultrahigh-field NMR spectrometers and increased interest in NMR studies of paramagnetic materials has placed a further emphasis on this subject. A significant amount of research effort has also gone into modifying polarization transfers involving commonly studied nuclides ($^{13}$C, $^{15}$N, $^{29}$Si, $^{31}$P, etc.) under MAS [20]. Many of these studies have focused on improving transfer efficiencies by altering the classical spin-locking scheme with ramped or adiabatic passage modulations of the RF profiles [21–24]. CP pulse sequences employing frequency swept spin-lock pulses to broaden the Hartmann–Hahn matching condition under magic-angle spinning have also been presented [25–33]; such experiments function in a similar manner to conventional CP experiments, in which spin polarization is produced in the transverse plane. Studies have also contemplated the effects and use of large anisotropic offsets [34]. However, improvements to the limited excitation bandwidth of conventional CP remains an open challenge in wideline NMR.

To address this, we discuss herein a CP experiment in which an adiabatic full passage is used in place of the conventional monochromatic $S$-nucleus spin-lock field. Since the characterizing feature of the resulting experiment is a polarization transfer using a *br*oadband *a*diabatic *in*version pulse, we have designated the pulse sequence BRAIN-CP. The application of adiabatic inversion pulses in BRAIN-CP provides two crucial characteristics: (i) the excitation profile is broad and uniform over bandwidths solely determined by the transmitting electronics, and (ii) the $S$-nucleus polarization is produced parallel (or anti-parallel) to the external field, which allows the magnetization to remain coherent across the broad powder pattern. A theoretical investigation of this polarization transfer process using average Hamiltonian theory and numerical simulations is presented. We also demonstrate the efficiency and broad excitation bandwidth of BRAIN-CP using $^{1}$H nuclei to polarize $^{119}$Sn, $^{199}$Hg and $^{195}$Pt nuclei in a series of chemically relevant samples. Furthermore, we demonstrate that BRAIN-CP can be used in conjunction with WCPMG signal acquisition, leading to a completely broadband experiment exhibiting multiplicative S/N gains.

## 2. Pulse sequence design

### 2.1. BRAIN-CP: overall considerations

The theory of adiabatic inversions on which this study is based is well known [35–39], so only a brief summary is presented before discussing their use in cross polarization. An adiabatic inversion can be brought about using a wide variety of pulse shapes (or by sweeping the external magnetic field), but the mechanism in all cases is similar. For simplicity we focus the discussion on a WURST pulse [14,40], which features a linear chirp of the effective transmitter offset frequency (associated with quadratic phase modulation of the radiofrequency, RF, pulse) and a slow rise/fall of the RF field amplitude at the beginning/end of the pulse (Fig. 1a). While the magnetic field generated by a monochromatic pulse appears stationary in the rotating frame defined by the transmitter frequency, the field generated by a frequency swept pulse only appears to stop rotating in the *xy* plane after a second rotational transformation applied at the instantaneous effective offset frequency; this shifting frame is normally referred to as the frequency
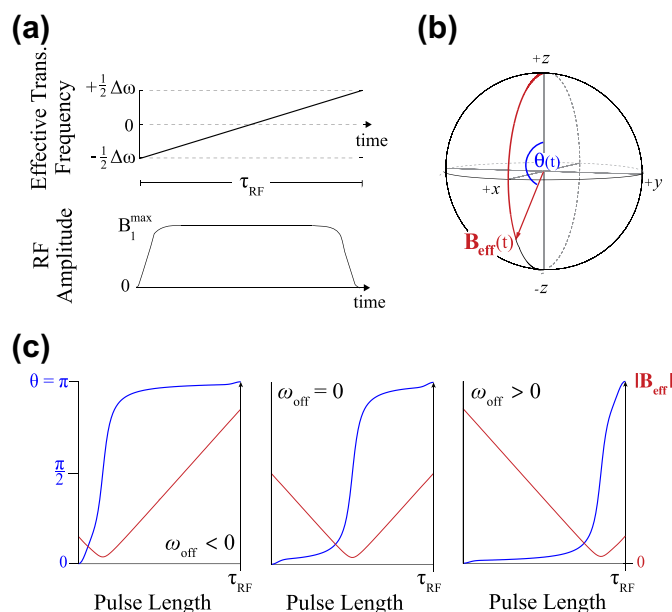


**Fig. 1.** Description of the WURST pulses used in this study as representative forms of adiabatic pulses highlighting (a) their effective transmitter frequency sweep and amplitude dependence versus time, and (b, c) the concomitant path taken by the effective magnetic field, $\mathbf{B}_{eff}$, during a typical adiabatic pulse as viewed in the FM frame. The behavior of the magnitude of $\mathbf{B}_{eff}$ (in red) and polar angle $\theta$ (in blue) is shown for cases where anisotropy shifts the resonance frequency of the spin to a lower frequency than the transmitter ($\omega_{off} < 0$), to a higher frequency ($\omega_{off} > 0$), or where the spin is on resonance ($\omega_{off} = 0$). $\mathbf{B}_{eff}$ is at a minimum when it crosses the transverse plane (i.e., $\mathbf{B}_{eff} = \mathbf{B}_1$ when $\theta = \pi 2$, which occurs at the point where the effective transmitter frequency equals the resonance frequency of the spin). (For interpretation of the references to color in this figure legend, the reader is referred to the web version of this article.)

modulated (FM) frame [36,37,39]. In this FM frame, the *z*-component of the effective magnetic field, $\mathbf{B}_{eff}$, varies with time because the instantaneous offset between the effective transmitter frequency and the resonance frequency of a given nucleus continuously changes (Fig. 1b). Typical $\mathbf{B}_{eff}$ trajectories for spins with different resonance frequencies (caused for instance by an anisotropic interaction) are shown in Fig. 1c. Although the details of these trajectories are different, a slow enough sweep of the effective transmitter frequency guarantees that spins initially polarized along the *z*-axis will remain locked along $\mathbf{B}_{eff}$ as it moves toward the $z < 0$ hemisphere; we note that only cases where the frequency sweep and amplitude modulation are such that the magnetization ends up aligned (or nearly aligned) along the $-z$-axis are discussed here.

While WURST pulses are typically employed for manipulating existing nuclear spin polarization, a coherence transfer application is explored herein in which the variable-amplitude, variable-angle $\mathbf{B}_{eff}$ generated by a frequency swept pulse is used as the spin-locking field in a modified CP experiment. The BRAIN-CP pulse sequence in Fig. 2a shows one possibility for applying this strategy. The $I = {}^{1}$H portion of the experiment is unchanged from the conventional CP experiment [17–19], while the contact pulse on the low-$\gamma$ $S$-spin channel is replaced with a chirped RF sweep applied to the anisotropically broadened target powder pattern (in principle different waveforms suited to a variety of conditions could also be utilized for the $I$ spins). The underlying rationale is foreshadowed in Fig. 1c (and further demonstrated below): at one or more points during the frequency sweep, a Hartmann–Hahn matching condition is fulfilled for each isochromat of the powder pattern. Polarization can then be transferred to $S$ nuclei regardless of their precise resonance offset, and magnetization will build up for every
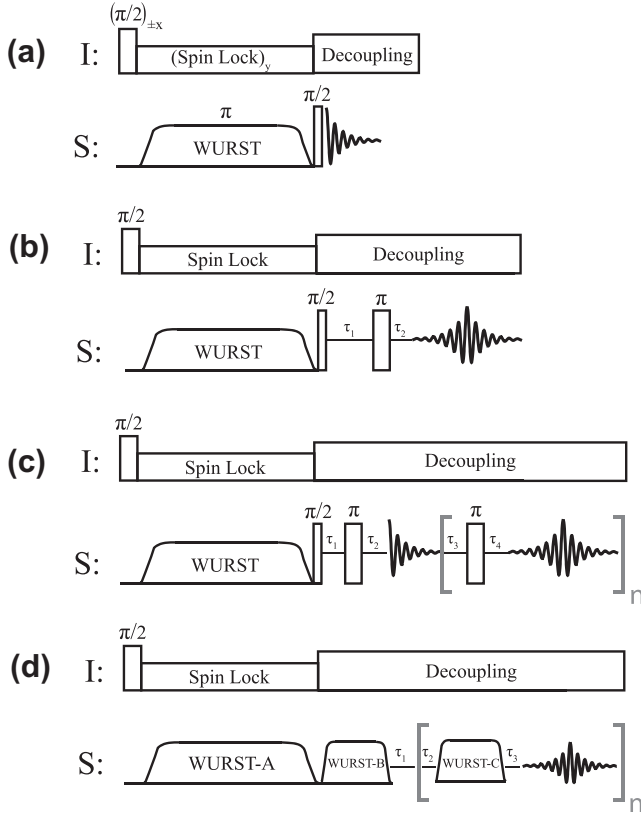
**Fig. 2.** Schematic pulse sequences for (a) BRAIN-CP, a cross-polarization sequence based on a broadband adiabatic full passage; (b) BRAIN-CP/echo, a version incorporating a hard π-pulse echo, (c) BRAIN-CP/CPMG, a multiple-hard-pulse echo version; and (d) BRAIN-CP/WCPMG, a fully broadband version of (c) which also incorporates adiabatic frequency sweeps during the acquisition period. These schematic representations assume a WURST envelope and a linear chirp—yet ample flexibility arises in these functions. See text for further details.

crystallite at some instant throughout the sweep. Once generated, the S-spin polarization adiabatically follows $\mathbf{B}_{\text{eff}}$, resulting in bulk spin polarization aligned along $-z$ for all sections of the powder pattern at the end of sweep. An S-channel π/2 pulse can be used to convert this polarization stored along $-z$ to observable transverse magnetization; we refer to this final pulse as the conversion pulse. Notice that the S-spin polarization can also be produced along $+z$, either by reversing the chirped pulse sweep direction or by phase-shifting the $^1$H excitation pulse by π with respect to the spin-lock pulse. This behavior was exploited by implementing a two-step phase cycle in all experiments, to filter out any initial S-spin polarization arising from thermal processes (which would lie along $+z$).

A variety of conversion pulses can be used to observe the $\pm S_z$ spin polarization produced by BRAIN-CP. For example, a single echo or a train of echoes can be acquired by using the BRAIN-CP-based sequences shown in Fig. 2b and c, respectively. The use of hard π/2 and π S-pulses, however, would deprive the ensuing sequences of their "broadbandedness." Alternatively, the $\pm S_z$ polarization produced by BRAIN-CP can be excited and observed using broadband methods—for instance, via the WCPMG pulse sequence in which the conversion and refocusing pulses are also frequency swept. An example of the resulting BRAIN-CP/WCPMG sequence is shown in Fig. 2d, where alphabetical labels denote the swept pulses used for polarization transfer (A), conversion (B) and refocusing (C). The BRAIN-CP/WCPMG pulse sequence allows for the S/N advantages of both CP and CPMG concurrently, providing broadband characteristics in both sections of the experiment.

## 2.2. Theoretical analysis: CP during an adiabatic pulse

We consider the effects of the pulse sequence shown in Fig. 2a on an isolated I,S spin pair during the contact period. The Hamiltonian may be defined in the doubly rotating frame, with spin I as the polarization source and spin S as the target:

$$H(t) = \Omega_I I_Z + \Omega_S S_Z + 2\omega_D I_Z S_Z + \omega_{1,I} I_X$$
$$+ \omega_{1,S}(t)[S_X \cos(\psi(t)) + S_Y \sin(\psi(t))] \quad (1)$$

Here, $\Omega_I$ and $\Omega_S$ are the rotating-frame resonance offsets of the I and S spins, $\omega_D$ is the dipolar coupling constant of the I,S spin pair, and the RF amplitudes applied to each spin are given by $\omega_{1,I}$ and $\omega_{1,S}$. The phase profile for the S channel RF is set according to the explicit form of a chirped pulse:

$$\psi(t) = \frac{Rt^2}{2} - \frac{\Delta\omega}{2}t + \psi_0 \quad (2)$$

which corresponds to an instantaneous RF frequency offset on that channel of

$$\omega_{RF}(t) = \dot{\psi}(t) = Rt - \frac{\Delta\omega}{2} \quad (3)$$

In these expressions, the time, t, runs from 0 to $\tau_{RF}$, $\psi_0$ is the initial RF phase, and the instantaneous irradiation frequency sweeps over the range $\Delta\omega$, from $\pm\frac{1}{2}\Delta\omega$ to $\mp\frac{1}{2}\Delta\omega$, at a rate $R = \Delta\omega/(\tau_{RF})$. Inclusion of a WURST-like amplitude profile could have an effect on the spin dynamics of S nuclei with offset frequencies that are close to the edges of the frequency sweep (i.e., when $\Omega_S$ is near $\pm\frac{1}{2}\Delta\omega$); however, we expect that most of the behavior is captured by treating $\omega_{1,S}$ as a constant.

After applying consecutive rotations to transform first to the FM frame [36] and then to the $\mathbf{B}_{\text{eff}}$ frame (i.e., to a frame which is tilted such that the new z axes are parallel to the effective magnetic fields influencing I and S) [37,39], the Hamiltonian can be expressed as

$$\widetilde{H}(t) = \Omega_I^{\text{eff}} I_Z + \Omega_S^{\text{eff}}(t) S_Z$$
$$- 2\omega_D[I_Z \cos(\theta_I) - I_X \sin(\theta_I)][S_Z \cos(\theta_S(t)) - S_X \sin(\theta_S(t))] \quad (4)$$

where the effective resonance frequencies of the I and S nuclei are

$$\Omega_I^{\text{eff}} = \sqrt{\Omega_I^2 + \omega_{1,I}^2}$$
$$\Omega_S^{\text{eff}}(t) = \sqrt{[\Omega_S - \omega_{RF}(t)]^2 + \omega_{1,S}^2} \quad (5)$$

The z axes of this $\mathbf{B}_{\text{eff}}$ frame subtend angles of $\theta_I$ and $\theta_S(t)$ with respect to the z-axes of a standard rotating frame, as described by

$$\cos(\theta_I) = \Omega_I/\Omega_I^{\text{eff}}$$
$$\cos[\theta_S(t)] = [\Omega_S - \omega_{RF}(t)]/\Omega_S^{\text{eff}}(t) \quad (6)$$

When the frequency sweep rate R is small, as in an adiabatic passage, the function $\theta_S(t)$ varies slowly and further time dependencies can be disregarded. Making the substitution

$$\widetilde{U}(t) = \exp\left\{-iI_Z\Omega_I^{\text{eff}}tI_Z - iS_Z\int_0^t \Omega_S^{\text{eff}}(t)dt S_Z\right\}\widetilde{\widetilde{U}}(t) \quad (7)$$

one obtains a Hamiltonian

$$\widetilde{\widetilde{H}}(t) = -2\omega_D\left[I_Z\cos(\theta_I) - I_X\sin(\theta_I)\cos\left(\Omega_I^{\text{eff}}t\right) - I_Y\sin(\theta_I)\sin\left(\Omega_I^{\text{eff}}t\right)\right]$$
$$\times \left[S_Z\cos(\theta_S(t)) - S_X\sin(\theta_S(t))\cos\left(\int_0^t \Omega_S^{\text{eff}}(t)dt\right)\right.$$
$$\left. - S_Y\sin(\theta_S(t))\sin\left(\int_0^t \Omega_S^{\text{eff}}(t)dt\right)\right] \quad (8)$$

An approximation to the dynamics can be obtained by considering the evolution of the spins under the average of Eq. (8)

$$\widetilde{\widetilde{H}}_{AV} = \frac{1}{\tau_{RF}} \int_0^{\tau_{RF}} \widetilde{\widetilde{H}}(t)dt \tag{9}$$

During the bulk of the irradiation period, the modulation frequencies $\Omega_S^{eff}(t)$ and $\Omega_I^{eff}$ impose fast oscillations on $\widetilde{H}$ and therefore make no contributions to the mean Hamiltonian. However, whenever $\Omega_S^{eff}(t) \cong \Omega_I^{eff}$, the integral of $\widetilde{H}$ may accumulate a nonzero value (see the Appendix A for further discussion of this criterion). This condition is analogous to the Hartmann–Hahn match [17], except that in the swept case the time-dependent match occurs at moments where the instantaneous frequency offset of the S-channel chirp fulfills the condition

$$\omega_{RF}(t) = \Omega_S \pm \sqrt{\Omega_I^2 + \omega_{1,I}^2 - \omega_{1,S}^2} \tag{10}$$

Assuming the abundant spins are on resonance, Eq. (10) describes a simple situation for the case where $\omega_{1,I} = \omega_{1,S}$: a polarization transfer occurs when the S-channel sweep is on-resonance with the S spin (i.e., when $\omega_{RF} = \Omega_S$). On the other hand, when $\omega_{1,I} > \omega_{1,S}$, polarization transfer occurs at two distinct positions in the sweep that lie on either side of the $\Omega_S$ resonance offset. It is also possible that a single match condition occurs when $\omega_{1,I} > \omega_{1,S}$, depending on the exact range of the RF sweep with respect to $\Omega_S$. The locations of these "match" criteria are further explored below with the aid of numerical simulations.

In order for this kind of broadband CP effect to be useful, it is important that the "matching" condition be maintained long enough for significant polarization to be transferred. Furthermore, for the experiment to be efficiently optimized, it is important to determine how the CP dynamics depend on each experimental parameter. It can be shown (see Appendix A) that if the effective RF fields on both channels are equal, cross polarization can occur at each $\Omega_S$ position during a time interval $\tau_{CP}$ given by

$$\tau_{CP} = \sqrt[3]{24\pi\omega_{1,S}/R^2} \tag{11}$$

It is more difficult to provide a simple estimate of the effective CP matching time when unequal RF fields are involved; still, in the $\omega_{1,I} \gg \omega_{1,S}$ case, this can be approximated as

$$\tau_{CP} = \sqrt[4]{\frac{16\pi^2}{R^2}\left(1 - \frac{\omega_{1,S}^2}{\omega_{1,I}^2}\right)} \tag{12}$$

Not surprisingly, a longer period of polarization transfer can be obtained by using either irradiation fields with $\omega_{1,S}^{max} = \omega_{1,I}$ or by sweeping through the S frequency offsets at a slower rate.

## 2.3. BRAIN-CP: numerical simulations

Numerical simulations of the behavior of an isolated I,S spin system during the contact portion of the BRAIN-CP experiment were also performed. Simulations are presented for an initial density operator $\rho(0) \propto I_X$ propagated numerically with the Hamiltonian in Eq. (1). All simulations are for a 10 ms chirped RF pulse swept at a constant rate from −75 to +75 kHz and a WURST-40 amplitude profile with a maximum RF power level $\omega_{1,S}^{max}/2\pi = 30$ kHz. In each simulation, the expectation values $\langle I_X \rangle(t)$ and $\langle S_Z \rangle(t)$ were calculated in order to monitor the polarization lost by spin I and gained by spin S during the contact period.

The polarization transferred under a range of I-channel RF power levels and S-spin frequency offsets is shown in Fig. 3. In each simulation, the point of polarization transfer from I to S is clear from the drop in $\langle I_X \rangle(t)$; the subsequent progression of the generated S magnetization toward the −z axis is also apparent. In
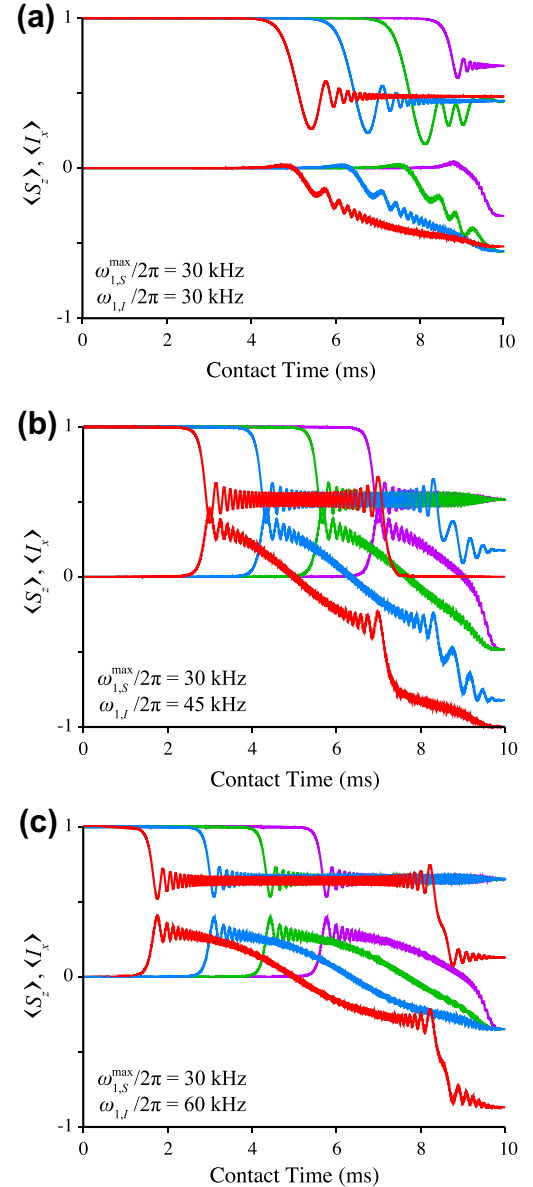


Fig. 3. Numerical simulations of polarization transfers for single I,S spin pairs during frequency-swept CP contact. Conditions for each simulation are: (a) $\omega_{1,I}/2\pi = \omega_{1,S}^{max}/2\pi = 30$ kHz, $\omega_D/2\pi = 0.5$ kHz; (b) $\omega_{1,I}/2\pi = 45$ kHz, $\omega_{1,S}^{max}/2\pi = 30$ kHz, $\omega_D/2\pi = 1.3$ kHz; and (c) $\omega_{1,I}/2\pi = 60$ kHz, $\omega_{1,S}^{max}/2\pi = 30$ kHz, $\omega_D/2\pi = 1.5$ kHz. For the initial conditions associated with each panel, results are calculated for anisotropic offsets $\Omega_S/2\pi = 0$ kHz (red), 20 kHz (blue), 40 kHz (green), and 60 kHz (purple), while $\Omega_I$ was set to 0 in all simulations. The transfer is monitored via calculation of the expectation values $\langle I_X \rangle$ and $\langle S_Z \rangle$, which are shown, respectively, at the top (with initial conditions $\langle I_X \rangle = 1$) and middle (initial conditions $\langle S_Z \rangle = 0$) of the frame. (For interpretation of the references to color in this figure legend, the reader is referred to the web version of this article.)

Fig. 3a, where $\omega_{1,S}^{max}/2\pi = \omega_{1,I}/2\pi = 30$ kHz, the simulations evidence a single polarization transfer that occurs at the point where the frequency of the RF sweep equals each S-spin frequency offset (i.e., when $\omega_{RF}(t) = \Omega_S$), in agreement with the prediction in Eq. (10). In Fig. 3b, where $\omega_{1,S}^{max} \neq \omega_{1,I}$, two separate polarization transfers are evident for the on-resonance $\Omega_S = 0$ case. By contrast, the same set of simulations shows that when $\Omega_S = 60$ kHz, a single transfer happens as only one of the two offset conditions of Eq. (10) ($\omega_{RF}(t)/2\pi = 60$ kHz $\pm$ 33.5 kHz) lies within the ±75 kHz range of the RF sweep. This behavior is further illustrated in Fig. 3c, where the larger difference in RF power levels is such that
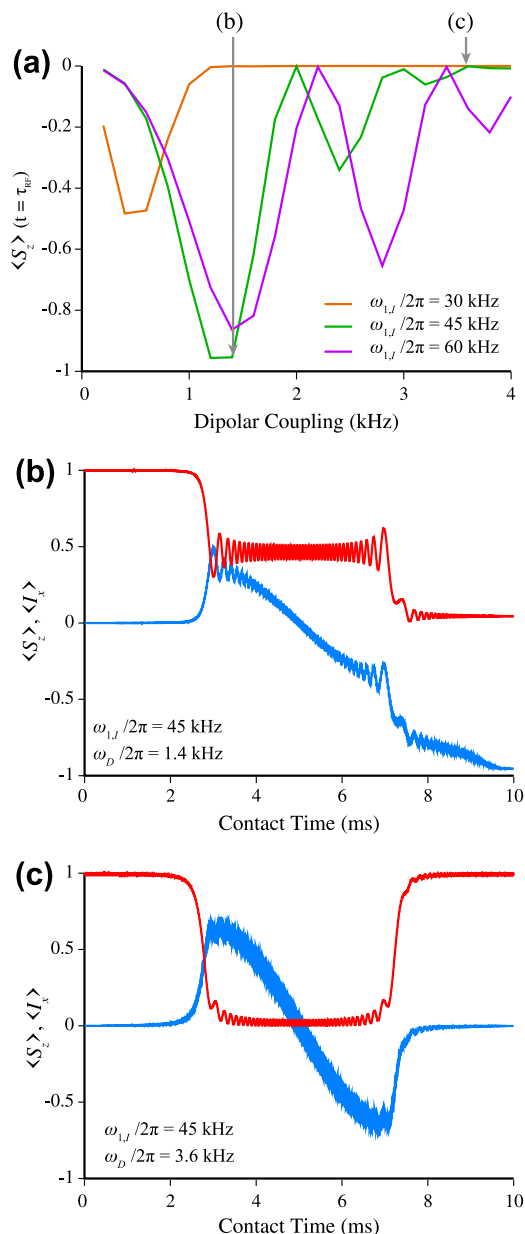
**Fig. 4.** Numerical simulations of the dipolar coupling dependence of polarization transfers for single $I,S$ spin pairs during BRAIN-CP. (a) Polarization transferred to the $S$ spin at the end of the contact pulse versus $I$–$S$ dipolar coupling constant, for three different RF power levels: $\omega_{1,I}/2\pi = 30$ kHz, $\omega_{1,S}^{max}/2\pi = 30$ kHz (orange); $\omega_{1,I}/2\pi = 45$ kHz, $\omega_{1,S}^{max}/2\pi = 30$ kHz (green); and $\omega_{1,I}/2\pi = 60$ kHz, $\omega_{1,S}^{max}/2\pi = 30$ kHz (purple). Two positions on the $\omega_{1,I}/2\pi = 45$ kHz curve displayed in panel (a) are expanded upon in (b) and (c), in which the time evolution of $\langle I_x \rangle$ (red) and $\langle S_z \rangle$ (blue) is shown in panel (b) for the dipolar coupling that yields the most complete transfer ($\omega_D/2\pi = 1.4$ kHz) and in panel (c) for the dipolar coupling that yields the least effective transfer ($\omega_D/2\pi = 3.6$ kHz). (For interpretation of the references to color in this figure legend, the reader is referred to the web version of this article.)

two polarization transfers are possible only when $\Omega_S$ is near the center of the sweep.

Effects of the magnitude of the $I$–$S$ dipolar coupling on the polarization transfers were also investigated. The $S$-spin polarization calculated at the end of the transfer period is shown in Fig. 4a as a function of $\omega_D$ under each of the three RF power conditions described above. The behavior under the lowest power setting clearly demonstrates that the polarization transfer is quenched when the dipolar coupling is higher than a certain threshold value. Most likely, this results from the spin-lock being maintained only when the RF power is of much greater magnitude
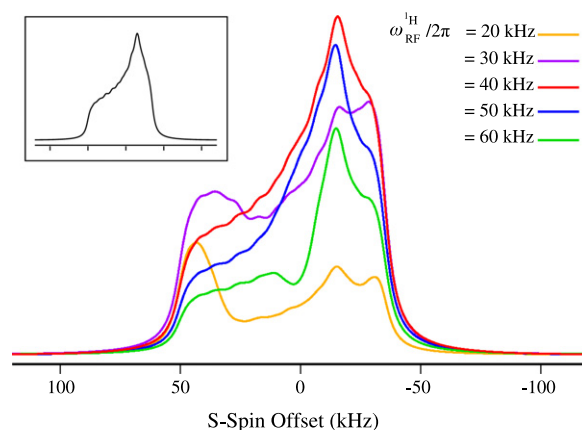


**Fig. 5.** Simulations of $^1$H-to-$S$ BRAIN-CP polarization transfers for an ABCX spin system with one $^{119}$Sn and three $^1$H nuclei, using SPINEVOLUTION [45]. For each simulation, $\omega_{1,S}^{max}/2\pi$ ($S$ = $^{119}$Sn) is 24.5 kHz while the value of $\omega_{1,I}$ ($I$ = $^1$H) is as listed in the figure. The model system has $S$-spin chemical shift tensor components: $\delta_{11} = 50$ kHz, $\delta_{22} = -12$ kHz and $\delta_{33} = -38$ kHz; three equivalent $\omega_D^{IS}/2\pi$ ($^1$H,$^{119}$Sn) values of 3.3 kHz; and $\omega_D^{II}/2\pi$ ($^1$H,$^1$H) values of 3, 3.7, and 21 kHz. The inset shows the idealized $S$-spin powder pattern, which is most accurately reproduced with BRAIN-CP when $\omega_1(^1$H)$/2\pi \approx 40$ kHz.

than all of the NMR interactions, including the dipolar coupling. The polarization transfer curves for $\omega_{1,I}/2\pi = 45$ and 60 kHz power levels display an interesting oscillation as a function of $\omega_D$ (Fig. 4a), representing efficient or inefficient polarization transfer at various points. The origin of this behavior is made clear by time-dependent simulations (Fig. 4b and c), expanding on the behavior at selected positions of the $\omega_D$-curve in Fig. 4a: the second of the two distinct transfer conditions associated with the frequency sweep may result in further polarization transfer from spin $I$ to spin $S$ (Fig. 4b), or in a reverse transfer, in which some or all of the polarization is returned to spin $I$ (Fig. 4c). Oscillatory shuttling of polarization back and forth between spins in an isolated spin pair is well known in conventional CP [41], but does not typically affect solid-state NMR spectra, as the oscillation is often dampened out by powder averaging or proton spin diffusion during long transfer periods [42–44]. Therefore, we expect BRAIN-CP to produce polarization transfers in a net $I$-to-$S$ direction under normal experimental conditions.

The analytical models also suggest that the effectiveness of the transfer may vary somewhat from crystallite to crystallite. This feature was investigated further with a series of numerical SPIN-EVOLUTION [45] calculations, probing the ability of BRAIN-CP to provide a faithful representation of a broad powder pattern dominated by chemical shift anisotropy (CSA). The model system was chosen to be an ABCX spin system comprising one $S$ and three $I = {}^1$H nuclei, including CSA effects for $S$ (modeled on $^{119}$Sn at 9.4 T), as well as both hetero- and homonuclear dipolar coupling (protons are assumed to be on resonance). The results of these simulations (Fig. 5) demonstrate that an accurate powder pattern is obtained when $\omega_{1,I}(^1$H$)/\omega_{1,S} \cong 2$. Under these conditions, the simulations indicate a polarization transfer equal to approximately half of the $\gamma_I/\gamma_S$ theoretical maximum. Given that this particular set of simulations only accounts for one of a multitude of possible spin systems and associated NMR parameters, we do not place much weight on this enhancement value; still, such simulations highlight the usefulness and validity of the pulse sequences presented here.

## 3. Experimental

The validity and potential usefulness of the proposed pulse sequences were investigated with an extensive series of

experimental tests. NMR spectra were acquired using a Varian Infinity Plus console and a 9.4 T Oxford magnet at resonance frequencies of 149.0 MHz for $^{119}$Sn, 83.5 MHz for $^{207}$Pb, and 71.4 MHz for $^{199}$Hg. All $^{119}$Sn experiments were performed using a Varian/Chemagnetics 4 mm HX MAS probe with samples packed in zirconia rotors, while $^{207}$Pb and $^{199}$Hg experiments employed a Varian/Chemagnetics 5 mm HX static probe and samples packed in glass tubes. Power calibrations at each frequency were performed using separate experiments with liquid solution standards. $^{119}$Sn spectra were referenced to liquid tetramethylstannane at 0 ppm, $^{199}$Hg spectra to a saturated aqueous solution of $Hg(ClO_4)_2$ at $-2253$ ppm (with respect to $Hg(CH_3)_2$ at 0 ppm), and $^{195}$Pt spectra to a 1 M aqueous solution of $Na_2PtCl_6$ at 0 ppm. All spectra were recorded using proton decoupling power levels of $\omega_1(^1H)/2\pi = 30$–50 kHz.

Simulations of polarization transfers were performed using either custom made routines written for Matlab or with SPINEVO-LUTION [45], as noted in the text. Analytical simulations of the total powder patterns were generated with WSOLIDS [46].

## 4. Results and discussion

### 4.1. $^{119}$Sn NMR experiments

$^{119}$Sn has a relatively high gyromagnetic ratio ($\nu_0 = 149$ MHz at 9.4 T) and often exhibits broad powder patterns arising from large CSAs [47], making $^{119}$Sn SSNMR an ideal starting point for testing the broadbandedness of our methods. Dibutyltin(IV) oxide, whose 110 kHz simulated static spectrum is shown in Fig. 6a [47,48], was employed as a test sample. Spectra acquired using conventional CP are displayed in Fig. 6b and 6c. The use of a high RF power for the match condition results in a successful enhancement of nearly the entire width of the powder pattern, whereas a low-power match results in excitation of only a fraction of the total powder pattern nearest to the transmitter frequency. Evidently, the low power condition is not optimal, but mimics samples spanning the ultra-wide bandwidths alluded to earlier. By contrast, the chirped BRAIN-CP approach successfully enhances the entire breadth of the powder pattern to the same S/N level as the conventional CP experiment, but without the need for high RF power levels (Fig. 6d). The contact-pulse sweep used in this example to provide the broadband CP transfer involved a WURST envelope and a carrier offset swept from just above to just below the spectral edges, covering a total range of 125 kHz. Interestingly, the same optimum RF power is found for the $^{119}$Sn contact pulse in both conventional CP and BRAIN-CP experiments when the amplitude of the $^1H$ contact pulse is fixed at $\omega_1/2\pi(^1H) = 20$ kHz for each experiment. Furthermore, the sensitivities to missets of the match power are found to be similar in both methods. There is a slight difference in the optimum contact times (5 ms for conventional CP versus 10 ms for BRAIN-CP). We ascribe the slower polarization transfer observed with BRAIN-CP to the frequency sweep bringing the RF pulse into contact with each isochromat of the powder pattern during only a portion of the total WURST pulse.

Given the success of BRAIN-CP in increasing the bandwidth of the polarization transfer, the viability of combining this process with CPMG-style acquisitions was tested. A conventional CP/CPMG spectrum, acquired under low-power CP matching conditions, is shown in Fig. 6e. While the initial $^{119}$Sn polarization generated by CP is equivalent, the S/N boost provided by the multi-echo acquisition of the CPMG loop allowed the CP/CPMG spectrum to be acquired using ten times fewer scans. The BRAIN-CP/CPMG spectrum shown in Fig. 6f, collected using identical pulse powers (and for the acquisition portions, equal timings) as the CP/CPMG spectrum, demonstrates the successful combination of broadband
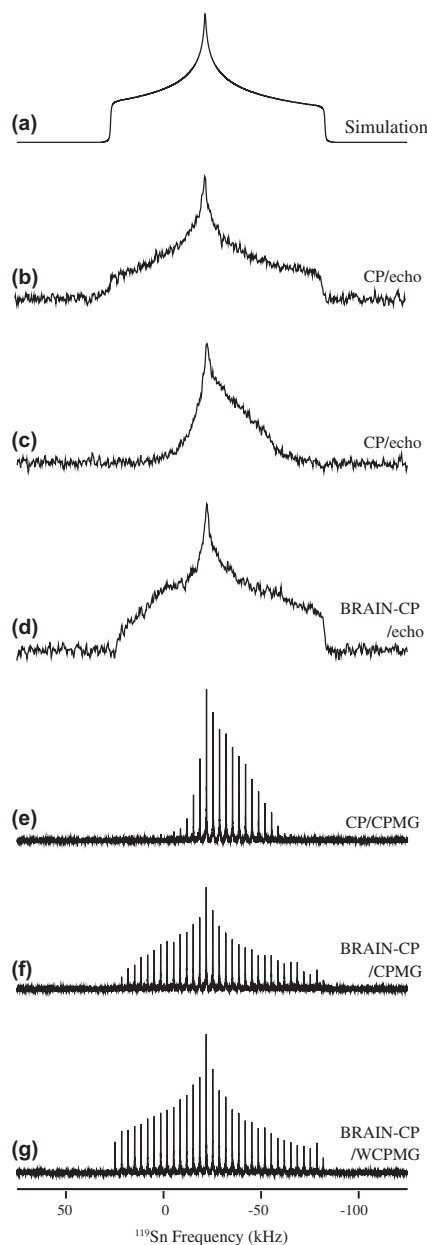


**Fig. 6.** $^{119}$Sn static NMR spectra of dibutyltin(IV) oxide. (a) Simulated spectrum based on literature chemical shift tensor parameters $\delta_{iso} = -173$ ppm, $\Omega = 737$ ppm (110 kHz at 9.4 T), and $\kappa = 0.12$ [47,48]; these values, and those in subsequent figures, are given using the Maryland convention [1]. (b, c) Echo spectra recorded using conventional CP with a 5 ms contact time. Spectrum (b) was acquired with a moderately high RF power [$\omega_{1,I}/2\pi(^1H) = 70$ kHz, $\omega_{1,S}/2\pi(^{119}Sn) = 65$ kHz], and (c) with a low RF power [$\omega_{1,I}/2\pi = 20$ kHz, $\omega_{1,S}/2\pi = 25$ kHz]. (d) BRAIN-CP/echo spectrum recorded using a 10 ms contact time with low RF powers identical to those employed for spectrum (c). The spectra presented in (b), (c) and (d) were recorded with 1024 scans using equivalent refocusing pulses and echo evolution periods. (e) CP/CPMG spectrum recorded using conventional CP with the contact time and RF powers set to equal those applied for the acquisition of spectrum (c). (f, g) Hard-pulse and swept-pulse CPMG echo variants of the BRAIN-CP experiment, with contact time and RF powers identical to those employed for the experiment displayed in (d). Conventional rectangular pulses used in the echo and CPMG experiments used $\omega_1/2\pi(^{119}Sn) = 55$ kHz, while the frequency-swept WURST-B (echo-train) pulses were swept over a range of 1 MHz with a power level of $\omega_1/2\pi(^{119}Sn) = 33$ kHz. The echo train spectra presented in (e), (f), and (g) were recorded using 128 scans of fifty 300 $\mu$s echoes.

polarization transfer with CPMG acquisition. Still, even for this test spectrum, the observable bandwidth is limited by the inversion profile of the rectangular $\pi$ pulses used in the CPMG train, as evidenced by the loss of intensity in the outer portions of the

CPMG-derived powder pattern. These distortions in the BRAIN-CP/CPMG spectrum highlight the need for broadband refocusing pulses in the CPMG train for the acquisition of broader powder patterns without distortions. The spectrum shown in Fig. 6g demonstrates that such broadband polarization/refocusing experiments are feasible if BRAIN-CP is used in conjunction with the S/N enhancement of the (also broadband) WCPMG method as shown in Fig. 1d. It is also interesting to note that this experiment appears to be quite robust, as doubling the contact-pulse sweep range to 250 kHz produces an indistinguishable BRAIN-CP/WCPMG spectrum (not shown), with approximately the same optimum $^{119}$Sn RF power, and a slightly longer optimum contact time of 15 ms.

## 4.2. $^{199}$Hg NMR experiments

Acquisition of $^{199}$Hg solid-state NMR spectra represents an even more difficult challenge for broadband CP experiments, as $^{199}$Hg has a lower gyromagnetic ratio than $^{119}$Sn (e.g., $v_0$ = 71 MHz at 9.4 T for $^{199}$Hg), and is often associated with CSA-dominated powder patterns that are thousands of ppm wide [47]. Mercury acetate has previously been used to demonstrate the benefits of combining conventional CP with the CPMG protocol [49,50], and is therefore a fitting sample with which to benchmark BRAIN-CP. The simulated ideal $^{199}$Hg powder pattern of mercury acetate (~130 kHz broad) is shown in Fig. 7a, together with the $^{1}$H–$^{199}$Hg CP/CPMG spectrum of mercury acetate in Fig. 7b. Despite the application of maximum RF power levels (acceptable for our equipment), the excitation profile of conventional CP covers only a portion of the total spectrum, in agreement with previous reports which found that six to nine CP/CPMG sub-spectra were required to obtain the entire powder pattern [49,50]. By contrast, the BRAIN-CP/WCPMG experiment yields the spectrum shown in Fig. 7c, where the broader excitation profile is evident. Similar to the $^{119}$Sn experiments, conventional CP and BRAIN-CP have nearly identical optimum match conditions, and also similar sensitivity to mis-setting of these power levels. Furthermore, the optimum contact time is again slightly longer for BRAIN-CP (25 ms), as compared to conventional CP (15 ms). We also note that a nearly identical spectrum (not shown) could be obtained using BRAIN-CP/WCPMG with a 500 kHz contact-pulse sweep width, a slightly longer contact time (30 ms) and a similar optimum RF power, suggesting that even extremely broad $^{199}$Hg powder patterns should be easily observable using this technique. Moreover, whereas a recent report has demonstrated that direct $^{199}$Hg excitation using the WCPMG sequence also allows for the acquisition of undistorted spectra of mercury acetate [16], this experiment was found to be quite inefficient due to the lack of signal enhancement from CP ($\sim\gamma_H/\gamma_{Hg}$) and the extremely slow $^{199}$Hg longitudinal relaxation: $5 \times T_1(^{199}$Hg$) \approx 25$ min. By comparison, the benefits of using BRAIN-CP/WCPMG are reflected in the fact that the spectrum in Fig. 7c, which is similar in quality to the direct excitation WCPMG experiments, was acquired ca. *50 times faster*.

## 4.3. $^{195}$Pt NMR experiments

As a final and particularly challenging test of the BRAIN-CP experiment, its use in $^{195}$Pt solid-state NMR spectroscopy was investigated. It is well known that spans of $^{195}$Pt chemical shift tensors are generally thousands of ppm in square planar environments [47,51], generating spectra that are hundreds of kHz broad on moderate and high-field NMR spectrometers. Pt[NH$_3$]$_4$Cl$_2$ exhibits these characteristics, and was used as a test sample. The $^{195}$Pt shift parameters of this compound are: $\delta_{iso}$ = −2540(60) ppm, $\Omega$ = 7250(100) ppm, and $\kappa$ = −0.96(1); further details of the NMR spectroscopy and its interpretation will be reported in a forthcoming publication. The $^{195}$Pt NMR spectrum of powdered Pt[NH$_3$]$_4$Cl$_2$ acquired using $^{1}$H–$^{195}$Pt CP/CPMG reveals that only a small fraction
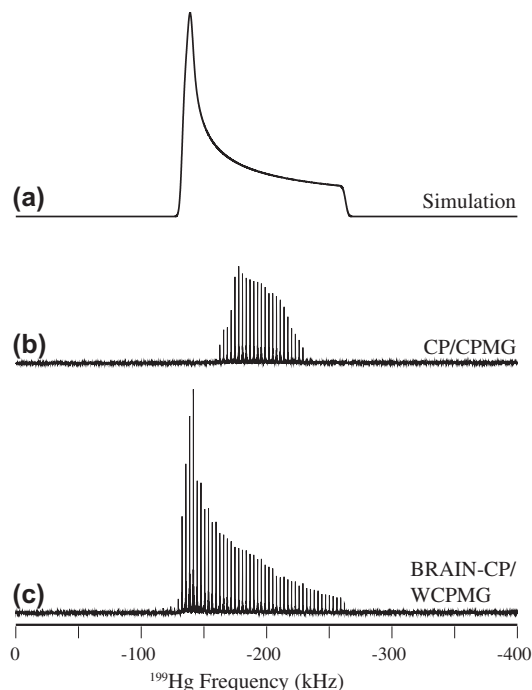


**Fig. 7.** Simulated and experimental $^{199}$Hg SSNMR spectra of mercury acetate. (a) Simulated spectrum based on the literature parameters $\delta_{iso}$ = −2496 ppm, $\Omega$ = 1850 ppm (131 kHz at 9.4 T), and $\kappa$ = 0.87 [49]. (b) CP/CPMG spectrum acquired with RF power levels of $\omega_{1,I}/2\pi(^{1}$H$)$ = 40 kHz and $\omega_{1,S}/2\pi(^{199}$Hg$)$ = 27.5 kHz during the 15 ms contact time and $\omega_1/2\pi(^{199}$Hg$)$ = 60 kHz refocusing pulses (c) BRAIN-CP/WCPMG spectrum acquired with a 250 kHz sweep and RF powers of $\omega_{1,I}/2\pi(^{1}$H$)$ = 40 kHz and $\omega_{1,S}^{max}/2\pi(^{199}$Hg$)$ = 30 kHz during the 25 ms contact time; 50 μs pulses swept over a range of 1 MHz at $\omega_1/2\pi(^{199}$Hg$)$ = 32 kHz were used for the WURST-B (echo-train) pulses. The spectra in both (b) and (c) were recorded using 16 scans of thirty 330 μs echoes.

of the approximately 600 kHz wide powder pattern is excited (Fig. 8a). Acquisition of the entire powder pattern using CP/CPMG at multiple transmitter positions was not attempted, but it is estimated that ca. 35 sub-spectra would be required. Obviously, the narrow excitation bandwidth of conventional CP is a severe impediment to $^{195}$Pt UW NMR spectroscopy.

The WCPMG spectrum of Pt[NH$_3$]$_4$Cl$_2$ in Fig. 8b demonstrates the broadband capability of this frequency swept acquisition method [51]; it also highlights the significantly lower signal intensity afforded by direct excitation in comparison to the CP/CPMG spectrum. In this case, the reduction in signal is due partly to the longer recycle delay associated with direct excitation (6 s) versus CP experiments (4 s) and the slightly poorer refocusing efficiency of the WURST pulses, yet the most important factor is the larger $^{195}$Pt spin polarization afforded by the CP experiment. We note that the short $T_1(^{195}$Pt$)$ for this sample is very unusual, with common longitudinal relaxation times and associated recycle delays being on the order of minutes; as a result, Pt[NH$_3$]$_4$Cl$_2$ is an excellent "setup" sample for both CP and non-CP $^{195}$Pt NMR experiments.

$^{195}$Pt BRAIN-CP/WCPMG spectra of Pt[NH$_3$]$_4$Cl$_2$, optimized using three different contact-pulse sweep widths, are shown in Fig. 8c–e. Experiments with all three contact-pulse sweep widths are found to require nearly identical power levels and optimal match conditions, and these are furthermore similar to the optimum power levels for the conventional CP experiment. It is immediately apparent from this data that the BRAIN-CP/WCPMG spectra provides a broader excitation while retaining the S/N advantages of CP. When a 1 MHz contact-pulse sweep width is applied, some signal intensity is excited over nearly the entire 600 kHz width of the spectrum, which is approximately 10 times the 60 kHz excitation
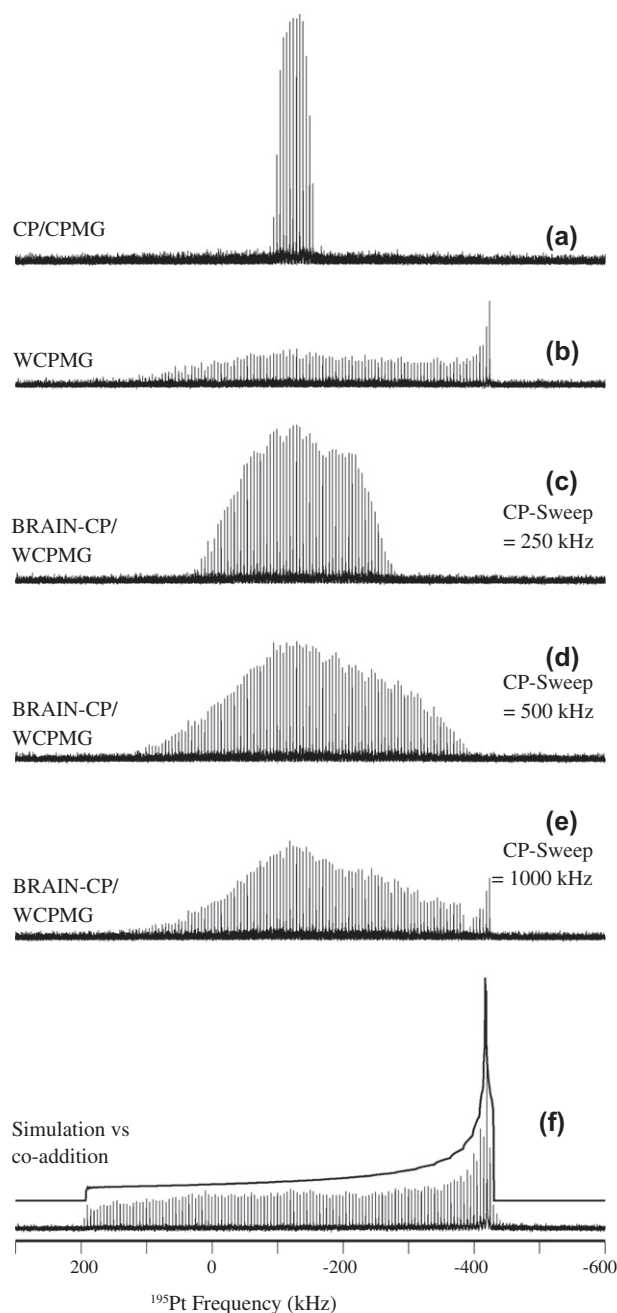
excitation and/or receiving bandwidths of the probe, rather than the performances of either the BRAIN-CP or WCPMG portions of the experiments. The same contact time was used for each experiment; however, it should be noted that no intensity was lost when a 10 ms contact time was used with the 250 kHz sweep, and memory limitations of the waveform generator prevented the investigation of contact times longer than 20 ms. Therefore, the behavior of the signal intensity as a function of contact time in these BRAIN-CP $^{195}$Pt experiments is not inconsistent with that found for the other nuclei. Given the extremely large excitation bandwidth of the BRAIN-CP/WCPMG pulse sequence, it is possible to obtain even the 650 kHz broad $^{195}$Pt spectrum of Pt[NH$_3$]$_4$Cl$_2$ using a small number of sub-spectra and a short total experimental time (Fig. 8f). It has been noted previously that the broadband refocusing of WCPMG makes it a preferred method over CP/CPMG for samples with characteristics similar to those of Pt[NH$_3$]$_4$Cl$_2$; the present results demonstrate that BRAIN-CP/WCPMG provides a further increase in efficiency. We also note that broadband direct $^{195}$Pt excitation experiments are often precluded by sample characteristics that are more challenging than those of Pt[NH$_3$]$_4$Cl$_2$: the sample may be available in limited quantities, have a dilute Pt content (Pt[NH$_3$]$_4$Cl$_2$ is nearly 60% Pt by weight), or possess unfavorable $^{195}$Pt relaxation properties (longer $T_1$($^{195}$Pt) and/or shorter $T_2$($^{195}$Pt) values than those of Pt[NH$_3$]$_4$Cl$_2$).

## 5. Conclusions

The BRAIN-CP pulse sequence, which uses frequency-swept adiabatic inversion pulses to achieve broad CP excitation profiles, has been introduced. Experimental results demonstrate that $^1$H nuclei can be used to polarize $^{119}$Sn, $^{199}$Hg and $^{195}$Pt nuclei with high efficiency over very broad frequency regions. In particular, the execution of CP along a spin-locking field in the FM-frame allows UW powder patterns to become uniformly polarized, leading to up to a tenfold reduction in the number of required scans in comparison to conventional CP experiments. Moreover, these experiments are found to require similar optimum RF power levels to conventional CP, and their spectral quality is relatively insensitive to changes in the contact-pulse sweep width or contact time. The detailed theoretical analysis provides insight into the behavior of the pulse sequence; as noted above, polarization transfer can occur when the S-channel offset creates an effective magnetic field equaling that experienced by the spin-locked $^1$H nuclei. Furthermore, we show that this transfer can be satisfied for most isochromats in broad powder patterns by sweeping the S-channel offset over a suitable range. This mechanism of polarization transfer leads to a large increase in bandwidth—not at the expense of power, but rather with the price of extended contact times. Experimental results demonstrate that the cost of this increase is well worth paying, making the ensuing BRAIN-CP sequence an attractive alternative for the polarization of CSA-broadened signals. The limits of the resulting bandwidths appear to be governed by the probehead's electronics rather than by spin-physics or waveform generating constraints. It is likely that the use of flat-Q circuits [52] could help overcome this particular hurdle. It is also worth noting the potential relevance of this scheme towards the polarization enhancement of quadrupole-broadened central and satellite transitions, as well as low-gamma nuclei. This aspect, together with extensions of BRAIN-CP analogues for the case of magic-angle spinning, is actively being investigated. Finally, it is important to note that it is the adiabaticity of the X-channel contact pulse that ensures a homogeneous magnetization transfer across the broad powder pattern. Therefore, the same basic mechanism for CP could be taken advantage of with a wide variety of alternate adiabatic inversion shapes beyond simple linear frequency chirps. The results obtained using BRAIN-CP and



**Fig. 8.** Experimental and simulated $^{195}$Pt NMR spectra of polycrystalline Pt[NH$_3$]$_4$Cl$_2$. (a) CP/CPMG spectrum acquired using RF power levels of $\omega_{1,I}/2\pi$($^1$H) = 47 kHz and $\omega_{1,S}/2\pi$($^{195}$Pt) = 27.5 kHz during the 5 ms contact time. Seventy-five 200 μs echoes were recorded using refocusing pulses with $\omega_1/2\pi$($^{195}$Pt) = 100 kHz. (b) Direct-excitation WCPMG spectrum acquired with 96 scans (128 scans were employed for all CP spectra to account for the 6 s recycle delay necessary for direct $^{195}$Pt excitation differing from the 4 s recycle delay of CP experiments). Seventy-five 200 μs echoes were recorded using 50 μs WURST-B pulses swept over 2 MHz at $\omega_1/2\pi$($^{195}$Pt) = 52 kHz. (c–e) BRAIN-CP/WCPMG experiments acquired using the indicated contact-pulse sweep widths, 20 ms contact times, and RF power levels of $\omega_{1,I}/2\pi$($^1$H) = 47 kHz and $\omega_{1,S}^{max}/2\pi$($^{195}$Pt) = 27.5 or 28.5 kHz. Each spectrum was recorded using identical echo train timings and refocusing pulse parameters to those employed in (b). (f) The total spectrum of Pt[NH$_3$]$_4$Cl$_2$ from the co-addition of 5 sub-spectra acquired by stepping the transmitter in 150 kHz intervals and employing 500 kHz contact-pulse sweep widths. The simulated spectrum is based on best-fit parameters $\delta_{iso}$ = −2540(60) ppm, $\Omega$ = 7250(100) ppm (620 kHz at 9.4 T), and $\kappa$ = −0.96(1) ppm.

bandwidth observed with conventional CP. In fact, the same excitation bandwidth as the extremely broadband WCPMG method is achieved. In this case the limiting factor is more likely the

frequency-swept WCPMG demonstrate high efficiency and ease of use, and the method shows clear promise for providing spectroscopic access to many nuclei with anisotropically broadened powder patterns in a wide array of materials.

## Acknowledgments

## Appendix A

We derive here an estimate of the time interval during which polarization transfer can occur using approximations to the equations for an isolated $I,S$ spin pair described in the *Theoretical Analysis* section of the main text. Polarization transfer is possible when the instantaneous RF frequency satisfies Eq. (10) of the main text; it therefore occurs within the sweep at time(s) $t_{CP}$

$$t_{CP} = \tau_{RF}\left(\frac{1}{2} + \frac{\Omega_S}{\Delta\omega} \pm \sqrt{\Omega_I^2 + \omega_{1,I}^2 - \omega_{1,S}^2}\right) \tag{A1}$$

provided that $0 \leqslant t_{CP} \leqslant \tau_{RF}$. Polarization transfer should then be possible during a certain interval around $t_{CP}$; an interval for which one can assume that the Hamiltonian in Eq. (8) is relatively unchanged. If the rapidly oscillating terms in Eq. (8) are neglected, this Hamiltonian can be written as

$$\widetilde{\widetilde{H}}(t) \cong -2\omega_D \cos(\theta_I)\cos(\theta_S(t))I_Z S_Z - \omega_D \sin(\theta_I)\sin(\theta_S(t))$$
$$\times \cos\left(\Omega_I^{eff}t - \int_0^t \Omega_S^{eff}(t)dt\right)(I_X S_X + I_Y S_Y) \tag{A2}$$

We note that the effective Hamiltonian in Eq. (A2) is similar to that for conventional CP; therefore, at long contact times, the maximum polarization increase for spin $S$ should equal the $\gamma_I/\gamma_S$ enhancement factor of conventional CP. Given that $\theta(t)$ is a slowly varying function the only oscillations in the ensuring dynamics will arise from the cosine term, whose phase is given by

$$\Phi(t) = \Omega_I^{eff}t - \int_0^t \Omega_S^{eff}(t)dt \tag{A3}$$

The change in $\Phi$ from $t = t_{CP}$ to $t_{CP} + t'$ is

$$\Phi(t_{CP} + t') - \Phi(t_{CP}) = \omega_{1,I}t' - \int_{\tau_{CP}}^{\tau_{CP}+t'} \Omega_S^{eff}(t)dt \tag{A4}$$

where for simplicity, we have taken $\Omega_I = \Omega_S = 0$. Expanding Eq. (A4) to third order as a Taylor series yields the phase change as

$$\Phi(t_{CP} + t') - \Phi(t_{CP}) = \pm\frac{1}{2}\sqrt{1 - \frac{\omega_{1,S}^2}{\omega_{1,I}^2}}Rt'^2 + \frac{1}{6}\frac{\omega_{1,S}^2}{\omega_{1,I}^3}R^2 t'^3 \tag{A5}$$

where the ± is related to the two possible match conditions of Eq. (10). In cases where $\omega_{1,I} = \omega_{1,S}$, the quadratic term in $t'$ vanishes and Eq. (A5) simplifies to

$$\Phi(t_{CP} + t') - \Phi(t_{CP}) = \frac{R^2 t'^3}{6\omega_{1,S}} \tag{A6}$$

We define phase changes in Eq. (A5) whose magnitude is smaller than $\pi/2$, as defining the approximate period during which the effective Hamiltonian (A2) varies little, allowing the mean Hamiltonian to build up and CP transfer to occur.

According to this analysis, when $\omega_{1,I} = \omega_{1,S}$, CP occurs during the interval $\tau_{CP}$ given by

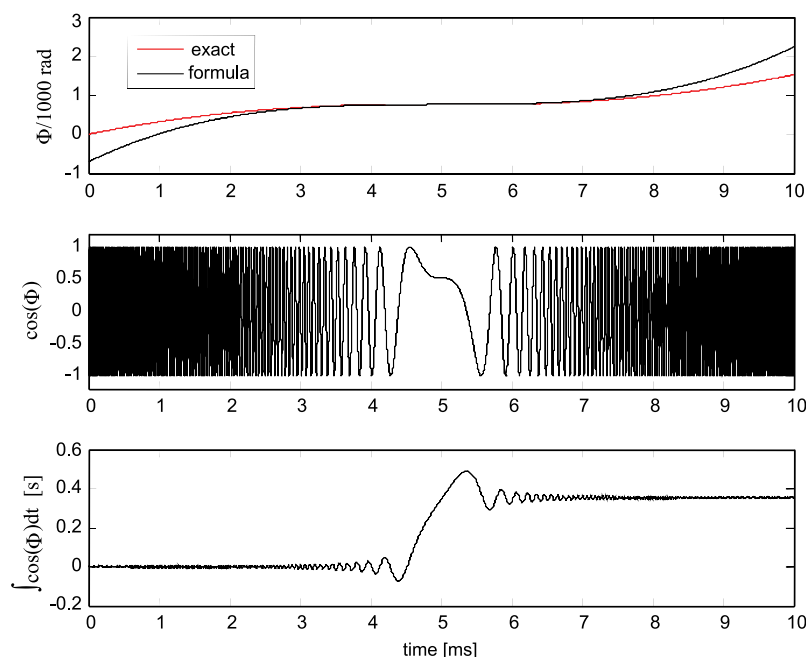$$\tau_{CP} = \sqrt[3]{24\pi\omega_{1,S}/R^2} \tag{A7}$$



**Fig. A1.** Graphs of the phase function $\Phi(t)$, as well as its cosine and integrated cosine functions, which govern the polarization transfer conditions, see text for further discussion.

To better illustrate the behavior, the phase function Eq. (A3) (and its cosine) are shown in Fig. A1 for a BRAIN-CP transfer with $\Delta\omega/2\pi = 150$ kHz, $\tau_{CP} = 10$ ms and $\omega_{1,I}/2\pi = \omega_{1,S}/2\pi = 20$ kHz. The period during which $\Phi(t)$ is relatively stable is apparent in the first panel, as are the rapid oscillations in $\cos[\Phi(t)]$ in the middle panel. It is only near the center portion of the sweep that the rapid oscillation of the cosine terms does not average to zero, and the integral of $\cos[\Phi(t)]$, rightmost panel of Fig. A1, only builds up during this time. Estimation of $\tau_{CP}$ directly from Fig. A1 gives $\tau_{CP} \cong 0.7$ ms, in excellent agreement with the estimation of 1.0 ms derived from Eq. (A7). A simple estimate analogous to Eq. (A7) is not possible when $\omega_{1,I} \neq \omega_{1,S}$; however, if $\omega_{1,I} \gg \omega_{1,S}$, the cubic contribution can be neglected such that the CP interval is approximated by

$$\tau_{CP} = \sqrt[4]{\frac{16\pi^2}{R^2}\left(1 - \frac{\omega_{1,S}^2}{\omega_{1,I}^2}\right)} \tag{A8}$$

For the case where $\omega_{1,I}/2\pi = 2 \times \omega_{1,S}/2\pi = 40$ kHz, $\Delta\omega/2\pi = 150$ kHz and $\tau_{RF} = 10$ ms, one gets $\tau_{CP} \cong 0.5$ ms which agrees with simulations performed for this matching condition. This analysis clearly demonstrates that contact between the spins is not an instantaneous moment, but rather occurs over a significant interval. We also note that the analysis presented is for a simple 2-spin system; $\tau_{CP}$ may be somewhat larger in real experimental systems, e.g., a range of $\Omega_S$ values would broaden the match condition.

## References

[1] M.J. Duer, Introduction to Solid-State NMR Spectroscopy, Blackwell Publishing Ltd., Oxford, UK, 2004.
[2] J.C.C. Chan, Solid-State NMR Spectroscopy, Springer-Verlag, Heidelberg, DE, 2012.
[3] R.W. Schurko, Acquisition of Wideline Solid-State NMR Spectra of Quadrupolar Nuclei, in: D.M. Grant, R.K. Harris (Eds.), Encyclopedia of Nuclear Magnetic Resonance, John Wiley and Sons, Chichester, UK, 2011. http://dx.doi.org/10.1002/9780470034590.emrstm1199.
[4] H.Y. Carr, E.M. Purcell, Effects of diffusion on free precession in nuclear magnetic resonance experiments, Phys. Rev. 94 (1954) 630.
[5] S. Meiboom, D. Gill, Modified spin echo method for measuring nuclear relaxation times, Rev. Sci. Instrum. 29 (1958) 688–691.
[6] S.E. Shore, J.P. Ansermet, C.P. Slichter, J.H. Sinfelt, NMR-study of the bonding and diffusion of CO chemisorbed on Pd, Phys. Rev. Lett. 58 (1987) 953–956.
[7] F.H. Larsen, H.J. Jakobsen, P.D. Ellis, N.C. Nielsen, Sensitivity-enhanced quadrupolar-echo NMR of half-integer quadrupolar nuclei. Magnitudes and relative orientation of chemical shielding and quadrupolar coupling tensors, J. Phys. Chem. A 101 (1997) 8597–8606.
[8] D. Massiot, I. Farnan, N. Gautier, D. Trumeau, A. Trokiner, J.P. Coutures, Ga-71 and Ga-69 NMR study of beta-Ga2O3 – resolution of 4-fold and 6-fold coordinated Ga sites in static conditions, Solid State Nucl. Magn. Reson. 4 (1995) 241–248.
[9] A. Medek, V. Frydman, L. Frydman, Central transition nuclear magnetic resonance in the presence of large quadrupole couplings: cobalt-59 nuclear magnetic resonance of cobaltophthalocyanines, J. Phys. Chem. A 103 (1999) 4830–4835.
[10] J.M. Böhlen, M. Rey, G. Bodenhausen, Refocusing with chirped pulses for broad-band excitation without phase dispersion, J. Magn. Reson. 84 (1989) 191–197.
[11] V.L. Ermakov, J.M. Böhlen, G. Bodenhausen, Improved schemes for refocusing with frequency-modulated chirp pulses, J. Magn. Reson., Ser. A 103 (1993) 226–229.
[12] R. Bhattacharyya, L. Frydman, Quadrupolar nuclear magnetic resonance spectroscopy in solids using frequency-swept echoing pulses, J. Chem. Phys. 127 (2007) 8.
[13] G. Kervern, G. Pintacuda, L. Emsley, Fast adiabatic pulses for solid-state NMR of paramagnetic systems, Chem. Phys. Lett. 435 (2007) 157–162.
[14] E. Kupče, R. Freeman, Adiabatic pulses for wideband inversion and broadband decoupling, J. Magn. Reson., Ser. A 115 (1995) 273–276.
[15] L.A. O'Dell, R.W. Schurko, QCPMG using adiabatic pulses for faster acquisition of ultra-wideline NMR spectra, Chem. Phys. Lett. 464 (2008) 97–102.
[16] A.W. MacGregor, L.A. O'Dell, R.W. Schurko, New methods for the acquisition of ultra-wideline solid-state NMR spectra of spin-1/2 nuclides, J. Magn. Reson. 208 (2011) 103–113.
[17] S.R. Hartmann, E.L. Hahn, Nuclear double resonance in the rotating frame, Phys. Rev. 128 (1962) 2042.
[18] A. Pines, J.S. Waugh, M.G. Gibby, Proton-enhanced nuclear induction spectroscopy – method for high-resolution NMR of dilute spins in solids, J. Chem. Phys. 56 (1972) 1776–1777.
[19] A. Pines, M.G. Gibby, J.S. Waugh, Proton-enhanced NMR of dilute spins in solids, J. Chem. Phys. 59 (1973) 569–590.
[20] F. Engelke, S. Steuernagel, Cross Polarization in Rotating Solids: Spin-1/2 Nuclei, in: D.M. Grant, R.K. Harris (Eds.), Encyclopedia of Nuclear Magnetic Resonance, John Wiley and Sons, Chichester UK, 2011. http://dx.doi.org/10.1002/9780470034590.emrstm0102.pub2.
[21] G. Metz, X.L. Wu, S.O. Smith, Ramped-amplitude cross-polarization in magic-angle-spinning NMR, J. Magn. Reson., Ser. A 110 (1994) 219–227.
[22] S. Hediger, B.H. Meier, R.R. Ernst, Adiabatic passage Hartmann–Hahn cross-polarization in NMR under magic-angle sample spinning, Chem. Phys. Lett. 240 (1995) 449–456.
[23] P. Hodgkinson, A. Pines, Cross-polarization efficiency in INS systems using adiabatic RF sweeps, J. Chem. Phys. 107 (1997) 8742–8751.
[24] M. Fukuchi, A. Ramamoorthy, K. Takegoshi, Efficient cross-polarization using a composite 0° pulse for NMR studies on static solids, J. Magn. Reson. 196 (2009) 105–109.
[25] A.C. Kolbert, A. Bielecki, Broad-band Hartmann–Hahn matching in magic-angle-spinning NMR via an adiabatic frequency sweep, J. Magn. Reson., Ser. A 116 (1995) 29–35.
[26] R.Q. Fu, P. Pelupessy, G. Bodenhausen, Frequency-modulated cross-polarization for fast magic angle spinning NMR at high fields: relaxing the Hartmann–Hahn condition, Chem. Phys. Lett. 264 (1997) 63–69.
[27] W.K. Peng, K. Takeda, M. Kitagawa, A new technique for cross polarization in solid-state NMR compatible with high spinning frequencies and high magnetic fields, Chem. Phys. Lett. 417 (2006) 58–62.
[28] W.K. Peng, K. Takeda, Efficient cross polarization with simultaneous adiabatic frequency sweep on the source and target channels, J. Magn. Reson. 188 (2007) 267–274.
[29] W.K. Peng, A. Samoson, M. Kitagawa, Simultaneous adiabatic spin-locking cross polarization in solid-state NMR of paramagnetic complexes, Chem. Phys. Lett. 460 (2008) 531–535.
[30] R.Q. Fu, J. Hu, T.A. Cross, Towards quantitative measurements in solid-state CPMAS NMR: a Lee-Goldburg frequency modulated cross-polarization scheme, J. Magn. Reson. 168 (2004) 8–17.
[31] H. Kim, T.A. Cross, R.Q. Fu, Cross-polarization schemes for peptide samples oriented in hydrated phospholipid bilayers, J. Magn. Reson. 168 (2004) 147–152.
[32] Y. Nishiyama, M.H. Frey, S. Mukasa, H. Utsumi, C-13 solid-state NMR chromatography by magic angle spinning H-1 T-1 relaxation ordered spectroscopy, J. Magn. Reson. 202 (2010) 135–139.
[33] K. Takeda, Y. Noda, K. Takegoshi, O. Lafon, J. Trebosc, J.-P. Amoureux, Quantitative cross-polarization at magic-angle spinning frequency of about 20 kHz, J. Magn. Reson. 214 (2012) 340–345.
[34] S.C. Shekar, D.K. Lee, A. Ramamoorthy, Chemical shift anisotropy and offset effects in cross polarization solid-state NMR spectroscopy, J. Magn. Reson. 157 (2002) 223–234.
[35] A. Abragam, The Principles of Nuclear Magnetism, Oxford University Press, Oxford, UK, 1961.
[36] J. Baum, R. Tycko, A. Pines, Broad-band and adiabatic inversion of a 2-level system by phase-modulated pulses, Phys. Rev. A 32 (1985) 3435–3447.
[37] A. Tannús, M. Garwood, Adiabatic pulses, NMR Biomed. 10 (1997) 423–434.
[38] M. Deschamps, G. Kervern, D. Massiot, G. Pintacuda, L. Emsley, P.J. Grandinetti, Superadiabaticity in magnetic resonance, J. Chem. Phys. 129 (2008) 204110.
[39] M. Garwood, L. DelaBarre, The return of the frequency sweep: designing adiabatic pulses for contemporary NMR, J. Magn. Reson. 153 (2001) 155–177.
[40] E. Kupče, R. Freeman, Stretched adiabatic pulses for broadband spin inversion, J. Magn. Reson., Ser. A 117 (1995) 246–256.
[41] G.C. Chingas, A.N. Garroway, R.D. Bertrand, W.B. Moniz, Zero quantum NMR in the rotating frame – J-cross polarization in AXN systems, J. Chem. Phys. 74 (1981) 127–156.
[42] L. Müller, A. Kumar, T. Baumann, R.R. Ernst, Transient oscillations in NMR cross-polarization experiments in solids, Phys. Rev. Lett. 32 (1974) 1402–1406.
[43] R.K. Hester, J.L. Ackerman, V.R. Cross, J.S. Waugh, Resolved dipolar coupling spectra of dilute nuclear spins in solids, Phys. Rev. Lett. 34 (1975) 993–995.
[44] W. Kolodziejski, J. Klinowski, Kinetics of cross-polarization in solid-state NMR: a guide for chemists, Chem. Rev. 102 (2002) 613–628.
[45] M. Veshtort, R.G. Griffin, SPINEVOLUTION: a powerful tool for the simulation of solid and liquid state NMR experiments, J. Magn. Reson. 178 (2006) 248–282.
[46] K. Eichele, R.E. Wasylishen, WSOLIDS, University of Alberta, Edmonton, 2000.
[47] T.M. Duncan, A Compilation of Chemical Shift Anisotropies, Farragut Press, Chicago, 1990.
[48] R.A. Komoroski, R.G. Parker, A.M. Mazany, T.A. Early, High-resolution Sn-119 NMR of some solid organotin compounds, J. Magn. Reson. 73 (1987) 389–398.
[49] I. Hung, A.J. Rossini, R.W. Schurko, Application of the Carr–Purcell Meiboom–Gill pulse sequence for the acquisition of solid-state NMR spectra of spin-(1)/(2) nuclei, J. Phys. Chem. A 108 (2004) 7112–7120.
[50] R. Siegel, T.T. Nakashima, R.E. Wasylishen, Application of multiple-pulse experiments to characterize broad NMR chemical-shift powder patterns from spin-1/2 nuclei in the solid state, J. Phys. Chem. B 108 (2004) 2218–2226.
[51] B.E.G. Lucier, A.R. Reidel, R.W. Schurko, Multinuclear solid-state NMR of square-planar platinum complexes – cisplatin and related systems, Can. J. Chem. 89 (2011) 919–937.
[52] G.D. Webber, P.C. Riedi, Broad-band NMR spectrometer for the study of hyperfine fields in ferromagnetic materials, J. Phys. E 14 (1981) 1159–1163.